ELSEVIER

www.elsevier.nl/locate/carres

Carbohydrate Research 326 (2000) 210–226

CARBOHYDRATE RESEARCH

Computational studies on carbohydrates: solvation studies on maltose and cyclomaltooligosaccharides (cyclodextrins) using a DFT/ab initio-derived empirical force field, AMB99C☆,☆☆

Frank. A. Momany *, J.L. Willett

Plant Polymer Research, USDA, ARS, National Center for Agricultural Utilization Research, 1815 N. University St., Peoria, IL 61604, USA

Received 15 September 1999; accepted 3 January 2000

Abstract

An empirical force field, denoted AMB99C, has been used to study molecular properties of α-(1→4)-linked carbohydrates in solution. AMB99C was parameterized using structural and energetic parameters from density functional ab initio methodology. In this work we examine the solution behavior of the β anomer of maltose and cyclohexa-, cyclohepta-, and cyclooctaamyloses (α-, β-, and γ-cyclodextrins or α-, β-, and γ-CDs, respectively), as well as of two larger (DP 10, ε-CD; DP 21) cyclomaltooligosaccharides, CA10 and CA21. Experimental data used for comparison purposes include X-ray structures, small-angle scattering radius of gyration values, NMR nuclear Overhauser enhancements (NOEs), and proton coupling constants. Molecular dynamics simulations were carried out using explicit water molecules (TIP3P) to establish equilibrium populations of conformations in solution, and these results are compared with other calculated values and a variety of experimental parameters, such as average H-1–H-4′ distances between the rings in β-maltose, and the primary hydroxyl groups' conformational populations. Medium-to-large cyclomaltooligosaccharide molecules were studied to test for glucose ring puckering and stability of kinked and 'flipped' conformations. The results of the solvation studies are in excellent agreement with experimental structural parameters. Published by Elsevier Science Ltd.

Keywords: Maltose; Cyclomaltooligosaccharides; Cyclodextrins; Conformation; AMB99C; Force field; Molecular mechanics; Dynamics

1. Introduction

In previous publications [1,2] a newly derived force field, AMB99C, was described and calculations on test molecules carried out in vacuo. It is common in the computational study of carbohydrates to use structural data obtained from crystallographic or NMR analysis as guides to the quality of theoretical computations. However, X-ray crystallographic data are limited to motions in the solid state, and no information is readily ob-

☆ Part III in the series, Computational Studies on Carbohydrates. For Part II, see preceding paper, Ref. [2].

☆☆ Names are necessary to report factually on available data; however, the USDA neither guarantees nor warrants the standard of the product, and the use of the name by USDA implies no approval of the product to the exclusion of others that may also be suitable.

* Corresponding author. Tel.: +1-309-6816362; fax: +1-309-6816362.

E-mail address: momanyfa@mail.ncaur.usda.gov (F.A. Momany)

0008-6215/00/$ - see front matter Published by Elsevier Science Ltd.
PII: S0008-6215(00)00043-4

tained that relates to conformational transitions occurring in the solvated state of the molecule. Carbohydrate NMR solution studies generally give limited data on average conformation because of the similarity of every sugar residue to every other sugar residue in the carbohydrate polymer. Therefore, to understand fully the solution dynamics and structure of a complex carbohydrate on the molecular level requires a computational method, such as molecular mechanics, to probe the energy states and dynamic motions in the environment of interest. From such computations one can attempt to explain the complicated atomic interactions that determine the conformational transitions ongoing in solution. The past decade has seen major advances in molecular mechanics techniques, particularly in molecular dynamics simulations using periodic boundary conditions, Monte Carlo searching methods, and distance cut-offs and switching functions to reduce the computational times, to name a few. Further, modern empirical molecular force fields have the potential to reproduce correctly most observable structural parameters in carbohydrates, if correctly parameterized. In this paper, we apply a new empirical force field, AMB99C, refined specifically for carbohydrates using results from DFT/ab initio geometry-optimized maltose conformers [1].

2. Methods

Nomenclature and software.—We use the recommendations and symbols of nomenclature as proposed by IUPAC [3] throughout. The relative orientation of a pair of contiguous glucose residues is described by two torsional angles at the glycosidic linkage, denoted ϕ and ψ. For a $(1\rightarrow4)$ linkage the definitions become those shown in Eqs. (1) and (2),

$$\phi = \text{O-5–C-1–O-1–C-4}' \text{ or}$$
$$\phi_{\text{H}} = \text{H-1–C-1–O-1–C-4}' \quad (1)$$
$$\psi = \text{C-1–O-1–C-4}'\text{–C-5}' \text{ or}$$
$$\psi_{\text{H}} = \text{C-1–O-1–C-4}'\text{–H-4}' \quad (2)$$

We use the following notations for the hydroxymethyl side chain orientations: (ω-1 and ωH-1) and (ω-1′ and ωH-1′) refer to the O-5–C-5–C-6–O-6 and C-5–C-6–O-6–H6 dihedral angles of the non-reducing residue, while the prime refers to the reducing sugar residue. These dihedral angles are often described as *tg*, *gg*, and *gt* for the rotation about the C-5–C-6 bond. The exo hydroxy groups used standard $\chi(i)$ notation.

Several different software programs were used to generate the carbohydrate three-dimensional structures. The MSI Polymerizer program (Molecular Simulations Inc., San Diego, CA) generates different linkages and specified configurations (L and D configurations as well as α and β anomeric configurations), as well as starting conformations (ϕ, ψ, ω and χ) of the sequences generated. A database of monosaccharide structures is available, and different linkages may be used during the building process. Using the MSI AmorphousCell program the radius of gyration of CA21 was calculated for comparison with experimental results. Atom typing and placing of atomic charges are carried out using the typing and charging algorithms in the MSI InsightII software. The rules for atom typing are the same used for the Homans [4] modified AMBER atom types, and the charges are applied to each atom through bond group charges, as described previously [2]. The force field is as described in Appendix A of Ref. [2].

Molecular mechanics calculations.—All calculations were carried out using the modified AMBER [5] force field, modified for carbohydrates, as described by Homans [4], and further modified, as described in Ref. [2] and denoted AMB99C. The new force field was implemented in the MSI InsightII/4.0 DISCOVER programs. The dielectric constant was treated as $\varepsilon = 1$ with the electrostatic and nonbonded van der Waals 1–4 terms scaled by 0.5. Empirical energy minimization was carried out to a gradient of less than ~ 0.001 kcal/mol using different minimization techniques, depending upon the size of the particular molecule or solvated system of interest. Molecular dynamics simulations were performed using the MSI DISCOVER program. Integration was numerically carried out using the Verlet algorithm, and trajectories were initiated by assigning velocity components, randomly selected from a thermal distribution

at 300 K, to the atoms. Calculations were carried out at 300 K with the temperature controlled by a weak coupling to a temperature bath. Time steps of 1 fs were used to calculate velocities, but results were stored for examination at picosecond intervals. The equilibration time was approximately 1/10 of the total simulation times, which varied from 100 to 800 ps in length. Explicit hydrogen atoms were included in all calculations, and both heavy atoms and hydrogen atoms were allowed to move on all molecules.

TIP3P water potentials were used throughout all simulations without internal constraints. For those calculations in which a periodic box was used to apply boundary and image conditions, the molecule was placed in a box, the size of which was determined by the size of the molecule and the number of water molecules desired. Water molecules were added to the box eliminating those overlapping with the substrate, and energy minimization was carried out. The explicit image model with cut-off distances of 12 Å and a switching function with a buffer width of 2 Å was used for water boxes. This method did not suffer from the 1/2 unit cell length for cut-offs that the simpler and faster minimum image method entails. After a short burst of molecular dynamics and more energy minimization, a second attempt to add more water was made to fill any holes or void volume not previously filled. This procedure was continued until the density within the box was correct for the system being studied. The pressure in the box was monitored at the end of the equilibrium stage of dynamics and adjusted by either adding or subtracting water molecules, changing the size of the box between runs, or running under constant pressure to adjust the volume conditions. If the density or pressure was not in the proper range after equilibration at constant volume, the simulation was stopped and restarted with the modified cell. The box sizes, solvent numbers, and dynamic time frames are listed in the tables for each individual run. Twelve different simulations with varying amounts of solvent, different lengths of time, various cut-off distances, and different cell sizes were examined as tests for convergence and equilibrium, but only several example runs are presented in the Tables here. We found no discernible differences in average conformation of maltose with large boxes and lots of water molecules or small boxes the size of crystallographic unit cells and only a few water molecules. The averaged results produced under constant pressure conditions were indistinguishable from the constant volume results.

Starting conformations to use in the solution dynamics simulations were obtained using a combination of dynamics simulations at elevated temperatures and structural preferences for allowed conformational space. Each minimum-energy bridge (ϕ, ψ) conformation of a disaccharide is associated with a manifold of minimum-energy conformations corresponding to different values of the exocyclic torsional angles. In the case of the primary $-CH_2OH$ groups, we adopted the preferred *gg* and *gt* conformers in vacuo and let the dynamic forces make the final decision as to the preferred position in solution. It was found in general that this group can undergo a rotational transition in solution and take up a preferred conformation, as do all the exocyclic hydroxyl groups throughout the molecules studied here. There may exist a residual conformational directing effect that is dependent upon the starting conformations, but this effect generally disappears shortly after a dynamics equilibration is achieved.

Adiabatic φ, ψ isopotential contour maps for a number of disaccaharides may be found in the literature, and these vacuum results will not be reproduced here, in particular because they have only limited interest when comparing conformational states in solution. Rather, we show several results of solution dynamics simulations where φ, ψ positions are plotted over the time of the simulation. The dynamics generated occupied φ, ψ maps describe in detail the allowed solution conformational energy–space regions.

3. Results and discussion

α and β anomers of maltose ('α- and β-maltose').—The AMB99C [2] potentials were tested by calculations of water solutions of maltose using a variety of experimental measurements as guides. Experimental data ana-

lyzed here include results from NMR experiments [6], as well as X-ray hydrate structures with well-defined solvent interactions. To provide information regarding β-maltose mean dihedral angles (i.e., the φ_H and ψ_H dihedral angles), and to examine the motions of this flexible molecule at moderate temperatures, molecular dynamics simulations were carried out in boxes of TIP3P water using a dielectric value of one. Reported here are runs of 100 ps (see Fig. 1), 300 ps and of 800 ps (see Fig. 2), carried out at 300 K on the β anomer. Two runs of 100 and 300 ps simulations were carried out on maltose (i.e., the α anomer) and are reported here. Many other runs, not reported here, were carried out to test for the effect of different water numbers, cell sizes, and cell shapes on the conformational preferences and backbone dihedral angles. As stated previously, we found no significant differences in average structures as a result of differences in numbers of solvent molecules or cell size and shape. Simulations are reported as average dihedral angles, average H-1–H-4′, O-4–O-1, and O-1–O-1′ distances, and average C–O–C bridge angles in Table 1. We found multiple population sites as have been found in previous studies with different force fields, but most of the abnormal transitions (i.e., to 'flipped' conformations for example) are very transitory. One result of the large (~ 2 kcal/mol) energy difference between the vacuum global minimum as fit to the DFT/ab initio results and the other minimum-energy conformations found from the B3LYP/6-31G* study is that a single popu-

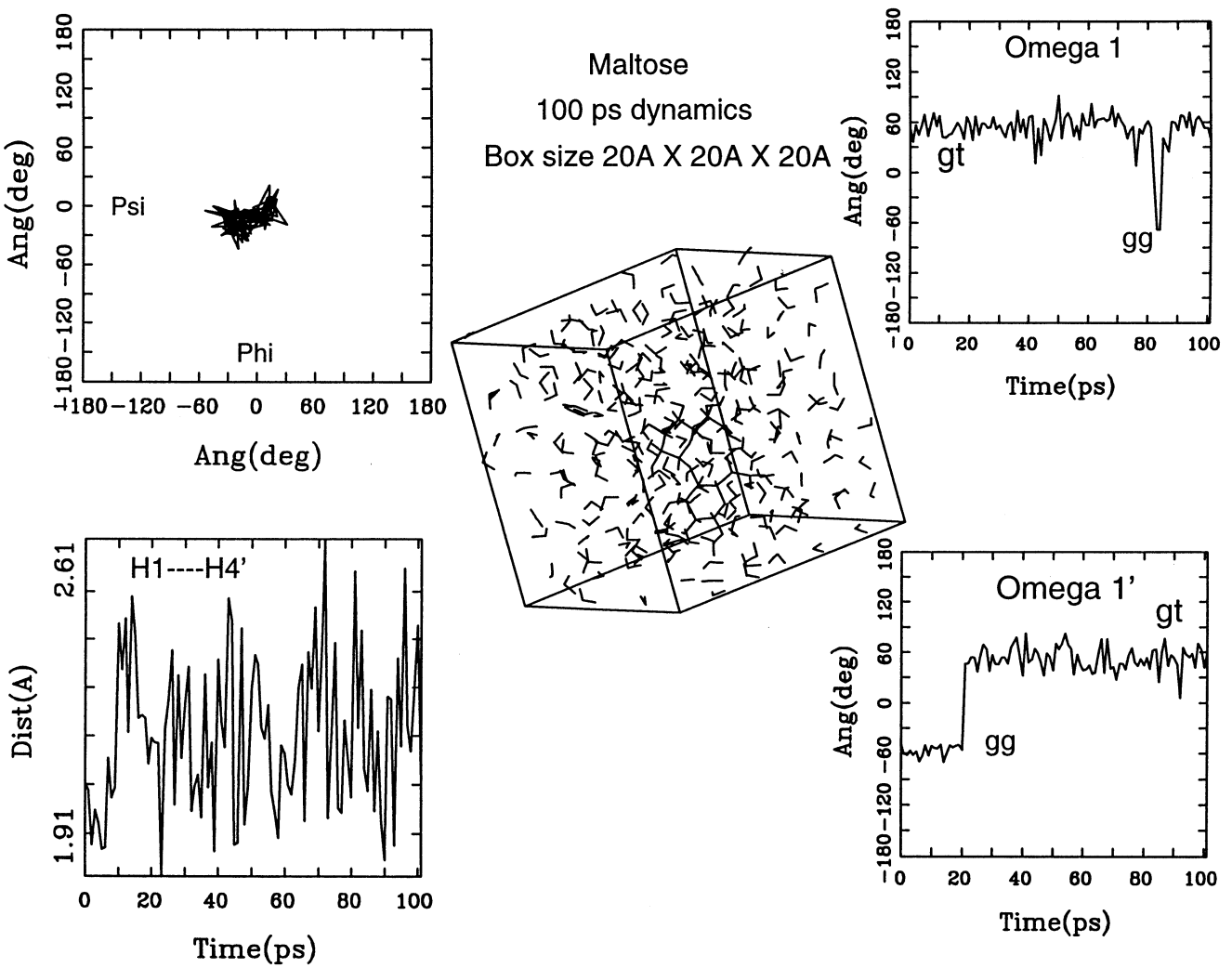

Fig. 1. Water–β-maltose dynamics analysis showing ϕ–ψ distribution over 100 frames of a 100 ps run, H-1–H-4′ distance, and torsional ωs vs. time.

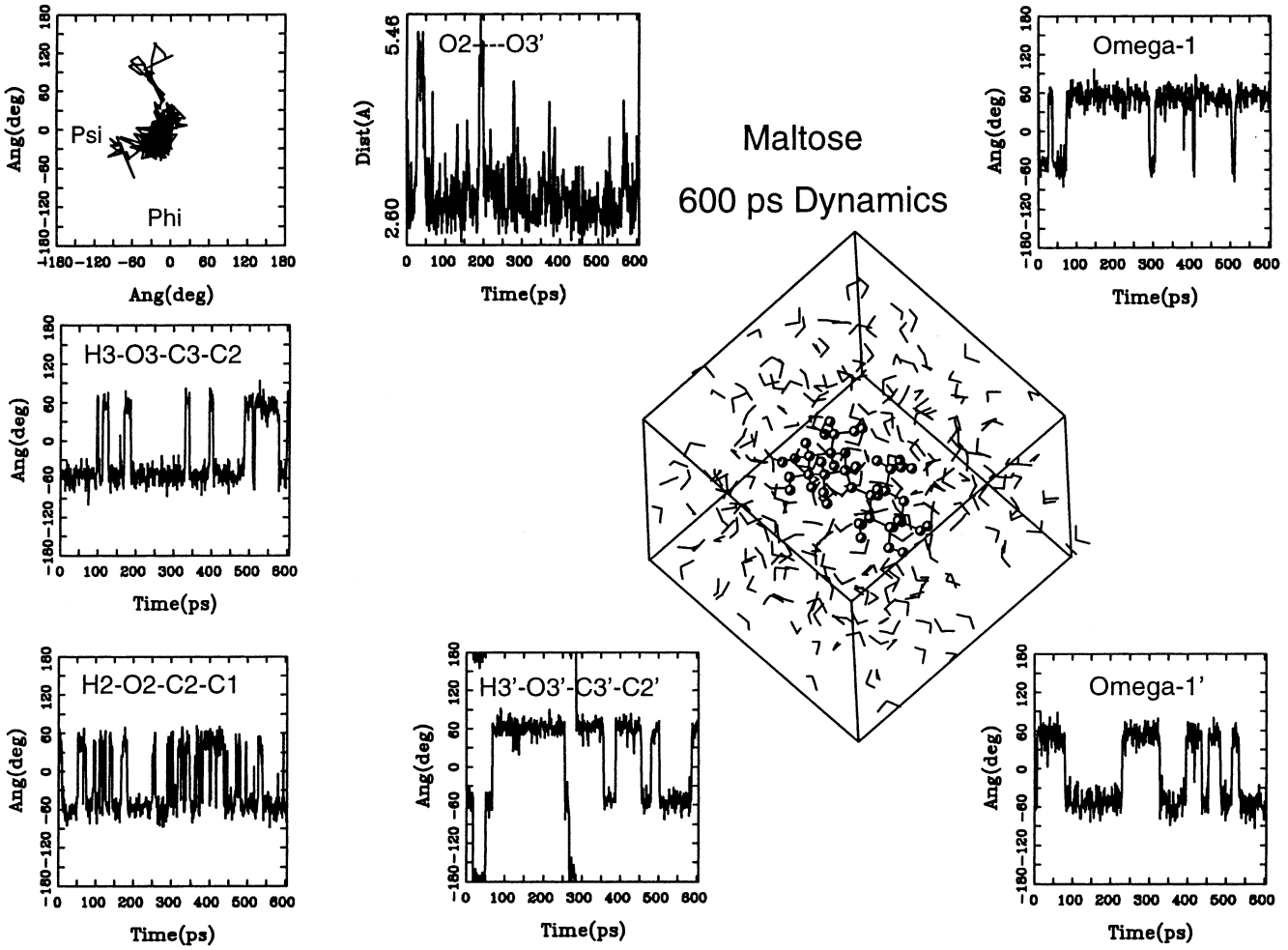

Fig. 2. Water–β-maltose dynamics analysis showing ϕ–ψ distribution over 600 ps of a 800 ps run (ring puckering occurred at 815 ps and the frames from 600–800 are not shown). The dihedral angles, H-3–O-3–C-3–C-2, H-2–O-2–C-2–C-1, H-3′–O-3′–C-3′–C-2′, and both ωs are shown vs. time. The O-2–O-3′ distances vs. time graph shows the few abnormal ϕ–ψ transitions as large values.

lated region is found during dynamics with other conformational states only sparsely populated. For example, simulation for 100 ps at 300 K of the 'flipped' conformation in water showed that the structure remained close to the starting conformation throughout the simulation, so at room temperature we did not observe a transition out of the second major minimum-energy conformation, showing that even in solution it is separated from the 'normal' conformational state by a fairly high energy barrier. This was even more apparent in the vacuum study [2] where a tighter range in the dynamic distribution of occurrences was observed in the φ–ψ map.

NMR experiments have provided evidence of ^{13}C–^{1}H coupling constants in the range of 2.5–4.5 Hz for $^{3}J_{CH}$, implying some difficulties in the measurements associated with concentration and temperature. Proton relaxation measurements give an average value for the H-1–H-4′ separation of 2.2–2.3 Å [6], compared with $\sim$2.1–2.2 Å from our dynamics calculations, consistent with the relatively small negative values of φ_H and ψ_H found here. The average value of the φ_H–ψ_H dihedral angles over the simulations reported here (see Table 1) are smaller than those derived by NMR studies, (i.e., $(-37, -33)$ [7], $^{3}J_{CH}=$ 3.6 and 4.0, respectively, and $(-29, -20)$ [6]; $^{3}J_{CH}=4.3$ and 4.9, respectively). Monte Carlo studies [7] suggested that the region with φ_H,ψ_H equal to $(-37, -33)$ was populated approximately 60–75% of the time, with larger negative values the rest of the time. Our results are not in agreement with that conclusion. From our calculations, values of φ_H and ψ_H, which are at the extreme ends of the

allowed conformations [8], that is, $\varphi_H \sim -60°$ and $\psi_H \sim -50°$, have H-1–H-4′ distances of 2.7–3.1 Å, much too large to be in agreement with those found by NOE studies. ^{1}H NMR [6,7] studies have agreed that the largest NOE is observed for H-1–H-4′, and that it is more than six times the value found for H-1–H-3′ [8]; it is this parameter that limits the extent that the backbone dihedral angles may take when averaged over the time of the experiment. This does not preclude transient excursions to larger negative values for φ_H and ψ_H during simulations.

Coupling constants for the φ_H and ψ_H dihedral angles have been measured by several authors. For example, Shashkov et al. [8] found $^3J_{H\text{-}1\text{–}C\text{-}1\text{–}O\text{-}1\text{–}C\text{-}4'}$ (J_ϕ) to be 3.5 ± 0.3 Hz and $^3J_{C\text{-}1\text{–}O\text{-}1\text{–}C\text{-}4\text{–}H\text{-}4'}$ (J_ψ) to be 3.9 ± 0.2 Hz for β-maltoside, whereas Gidley [9] reports a J_ϕ of 4.5 Hz and J_ψ of 4.5 Hz for maltose in D_2O. These differences may be a result of the different concentrations studied. However, using

Table 1
Average dihedral angles, average H-1–H-4′ distance, average C–O–C angle, and average O-4–O-1 and O-1–O-1′ distances for α- and β-maltose from dynamics simulations in water[a]

Run #	Average dihedral (°)		H-1–H-4′ distance (Å)	Angle C-1–O–C-4′ (°)	O-4–O-1 distance (Å)	O-1–O-1′ distance (Å)
	ϕ_H	ψ_H				
β Anomer						
I 300 ps, TIP3P	−15	−20	2.1	119	4.51	5.25
Cell size 20×20×20 Å, 244 water molecules						
Min	−1	0	1.9	112	4.41	5.08
Max	−35	−41	2.5	125	4.61	5.48
II 800 ps, TIP3P	−18	−15	2.1	119	4.43	5.24
Cell size 20×20×20 A, 244 water molecules						
Min	−7	−1	1.9	111	4.03	4.72
Max	−97 [b]	−75 [b]	2.3	127	4.63	5.45
III 100ps, TIP3P	−18	−18	2.1	119	4.42	5.23
Cell size 15×15×15 AÅ, 86 water molecules						
Min	−1	0	1.9	111	4.16	4.87
Max	−52	−45	2.8	125	5.11	5.65
Average of β	−17	−18	2.1	119	4.45	5.24
α Anomer						
IV 300ps, TIP3P	−16	−18	2.2	118	4.56	4.56
Cell size 20×20×20 Å, 244 water molecules						
Min	0	0	1.8	112	4.00	3.83
Max	−25	−36	2.8	122	5.24	5.16
V 100ps, TIP3P	−13	−14	2.1	119	4.45	4.49
Cell size 15×15×15 Å, 86 water molecules						
Clockwise exocyclic hydroxyl						
Min	0	0	1.9	110	4.22	4.01
Max	−27	−36	2.5	126	5.06	5.24
Average of α	−15	−16	2.2	119	4.50	4.53

[a] A small population of (+.+), (+.−) and (−.+) conformations are found during the dynamic simulation, but are not included in the average values.

[b] Abnormal conformations (i.e., large negative values of ϕ and ψ are not included in the min and max values for the other parameters.

the Karplus equation for C–O–C–H derived for a series of model compounds having the O–C–O motif [10] as in Eq. (3):

$$^3J_{C-H} = 5.7\cos^2 F - 0.6\cos F + 0.5 \quad (3)$$

where F is the dihedral angle between the vicinal hydrogen and the carbon in the C–O–C–H arrays of bonded atoms, we obtain J_φ and J_ψ values for the averaged maltose simulated conformations of 5.1 and 5.1 for ϕ_H, $\psi_H = (-17°, -18°)$. Our calculated values for the coupling constants are larger than the experimental values obtained by Gidley [9], but they do not include those dihedral angles that make up a small percentage of the population and would tend to lower the calculated coupling constants. For example, a small population of the 'flipped' state ($-20°$, $-140°$; $J_\phi = 4.9$, $J_\psi = 4.3$ Hz) would result in lowering both calculated coupling constants to give better agreement with experiment. It is of interest that Mulloy et al. [11] found the Karplus equation for C–O–C–H to be

$$^3J_{C-H} = 5.5\cos^2 F - 0.7\cos F + 0.6 \quad (4)$$

using different model compounds to fit the coefficients. Using Eq. (4), we obtain coupling constants ~ 0.2 smaller in value than those obtained from Eq. (3), which are in even better agreement with experimental values when corrected for minor populations of conformations. It is important to note that the experimental coupling constants imply nearly equal values for ϕ and ψ, and the calculations reported here are in agreement with that finding.

It is also possible to note that the use of several short simulations resulted in the same average values for molecular parameters as found from longer (~ 800 ps) simulations. Each run was started from a different system state (usually after energy minimization of the last frame of a previous run) and different random number seed. No differences were found that would indicate that the starting conformation biased the resulting dynamics averages over 100–200 ps simulation in water with the exception of one simulation (see Fig. 3) in which the clockwise direction of the exocyclic hydroxyl groups was used as the starting structure. This simulation of 100 ps resulted in the preservation of some of the clockwise torsional terms up to ~ 20 ps, so one should be aware of the time factor for this interconversion and give ample simulation time for the molecule to reach full equilibrium. The fact that the time factor is important can also be seen in the conformational transitions about the ωs. The 100 ps simulation in Table 1 does not show many gg/gt transitions for either ring; however, the 600 ps graphs show that such transitions occur, but occasionally they remained in one conformation over long (~ 100 ps) time periods. The ω and ω' transitions are described in detail later in this section.

Previous simulations with the GROMOS force field [12,13] reached considerably different average structures from water simulations. The average ϕ_H and ψ_H values for several different dynamic simulations [12,13] in different numbers of water molecules were as follows: ($-41°$, $-28°$) with 499 waters, ($-46°$, $-34°$) with 499 waters, ($-44°$, $-34°$) with 137 waters, ($-53°$, $-26°$) with 137 waters, and ($-22°$, $-21°$) with 137 waters. The in vacuo average ϕ_H, ψ_H result with the modified GROMOS force field was ($-20°$, $-17°$). The authors [12,13] report that about 20% of the conformational population of one run was characterized by positive ϕ_H and ψ_H values, in disagreement with the results presented here and with the results of the vacuum DFT/ab initio study [1] in which no minimum energy conformation was found in the ($+$, $+$) region of ϕ_H–ψ_H space. It appears that the dihedral angles described using the GROMOS force field may also be in a more negative region of space than the observed NMR H-1–H-4′ distances would suggest, because larger negative averages for ϕ_H and ψ_H result in a calculated average H-1–H-4′ distance of ~ 2.6 Å, and that value is significantly larger than the 2.2–2.3 Å obtained in the NMR results cited above. Glennon et al. [14] published a revision of AMBER in which the in vacuo isoenergetic potential energy map gave minima at ($-40°$, $-40°$) and (20°, 20°). These results are again not in agreement with the vacuum study or solvated simulations reported here.

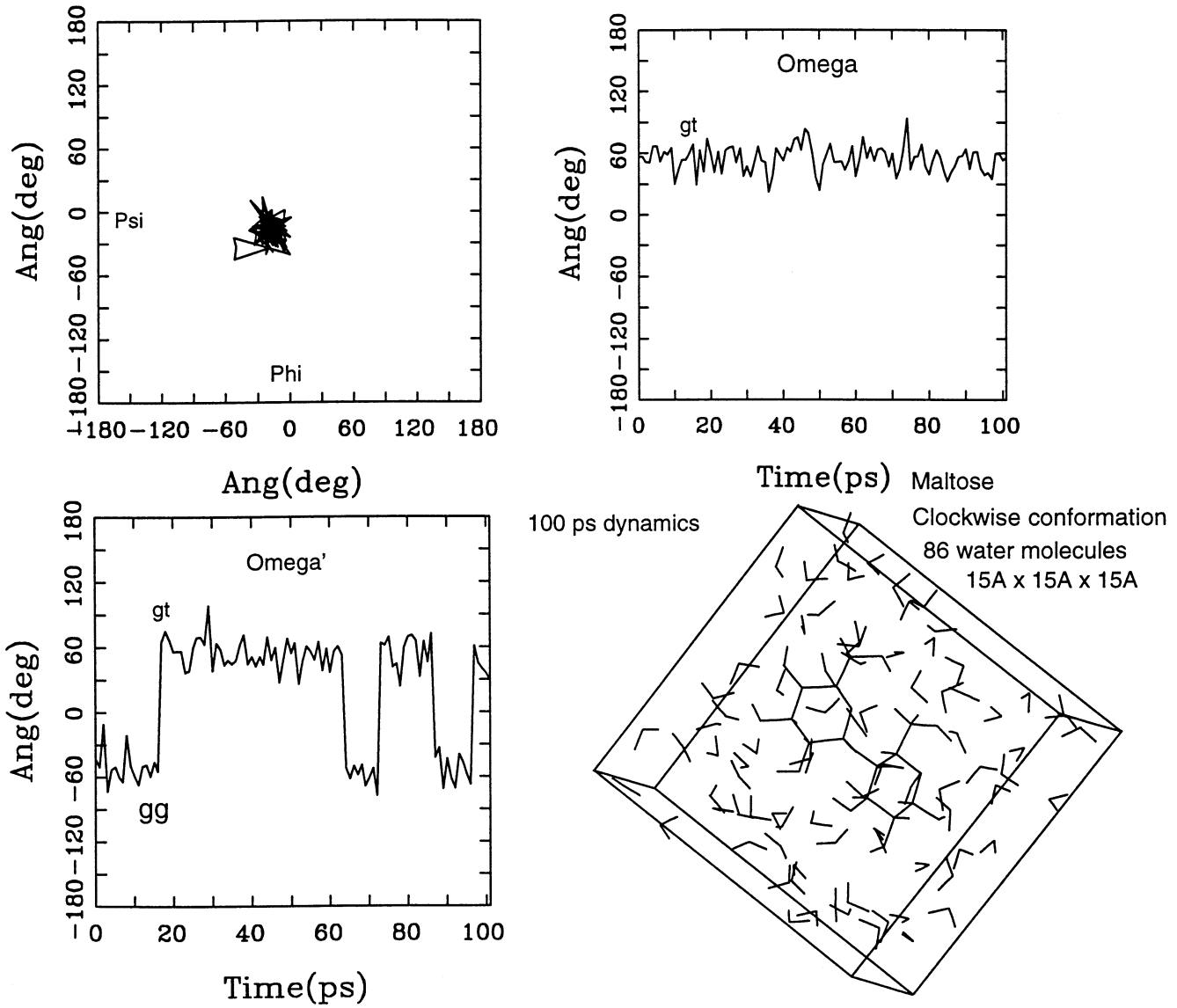

Fig. 3. Water–β-maltose dynamics analysis for a conformation with 'clockwise' orientation of the exocyclic hydroxyl groups. The ϕ–ψ distribution is very tight over 100 ps of dynamics.

Finally, the maltose–water simulation of Brady and Schmidt [15] is compared with the results presented here. Their vacuum-averaged mean values for ϕ_H and ψ_H were ($-58°$, $-44°$) and (32°, 16°), while their average values in solution were ($-62°$, $-49°$) and (28°, 20°). Neither of these two wells is a low-energy minimum in the AMB99C force field. The partial charges used [15] are very similar to those employed here (see Fig. 2) and should closely reproduce the interaction energies with the TIP3P water molecules. To this end we find similar numbers of hydrogen bonds formed between water and β-maltose as did Brady and Schmidt [15]. Both force fields use a dielectric constant $\varepsilon = 1$ [15] so we would not expect that the hydrogen-bonding energies and geometric patterns would change significantly. Brady and Schmidt [15] reported a trajectory result obtained after reducing the charges on the hydroxyl oxygen atoms from -0.65 to -0.55 esu and after reducing some carbon atoms by 0.05 to 0.10 esu. They did not change the charge on the hydroxyl hydrogen atoms. The result of this change in partial atomic charge was the occurrence of conformational transitions between the different low-energy wells, which were not observed previously. In particular, they reported excursions to ($-62°$, $-49°$) from their B ($-$, $-$)

well during which the internal O-2···O-3′ hydrogen bond was broken and exchanged for hydrogen bonds to the solvent. We observe (AMB99C) that this exchange takes place routinely in the current low-energy well. However, this hydrogen-bond breaking process is not simply due to a rotation about the φ_H and ψ_H dihedral angles, but is a function of the rapid rotation of the hydroxyl hydrogen atoms at the O-2 and O-3′ sites. From Fig. 2 it is clear that rotation about the C-2–O-2 and C-3′–O-3′ bonds does not show a coupled correlation for gauche or trans conformations between these interacting pairs. This suggests that the interaction of these two hydroxyl groups with the solvent is playing an important role relatively independently of the linkage conformation. Finally, the observation by Brady and Schmidt [15] that with the reduced charges the average dihedral angles for φ_H and ψ_H are more localized in the B well ($\sim -20°$, 0°) is in better agreement with our results.

With respect to the partial charges used in this work, a comparison of a recent OPLS parameterization of carbohydrates [16] is useful. The partial atomic charges of the O and H atoms of the alcohol groups in Ref. [16] were taken to be -0.683 and 0.418 esu, respectively. These compare favorably with the -0.650 and 0.430 esu used for the exocyclic hydroxyl groups in this work. Damm et al. [16] used -0.40 esu for the ether oxygen, while we used -0.20 esu.

Finally, we examine the population of 6-position primary alcohols from the simulations. Recent experimental studies find an average population of *gg*/*gt*/*tg* conformations of $\sim$ 60:40:0 [17] for the reducing sugar in maltose. We find (see Fig. 2) a complicated pattern of conformational preferences, with the non-reducing end preferring the *gt* for $\sim 85\%$ of the time with *gg* $\sim 15\%$ and *tg* very transitory. The reducing sugar favors the *gg* for $\sim 60\%$ of the time with *gt* $\sim 40\%$ of the time, which is in excellent agreement with the NMR results [17] noted above. In every maltose simulation we find this population difference between the two rings, even though the parameters for torsional energy and all other force field terms are identical at the C-5–C-6 and C-5′–C-6′ bonds. It is clear that this result complicates the experimental NMR analysis, but none the less the calculated results are very encouraging. As can be seen in Fig. 2, the O-2–O-3′ distance fluctuates from the shortest interaction of 2.60 Å up to 5.46 Å, with most of the population being in the ~ 3.0 Å range. However, the direction of the H-2–O-2 bond relative to the direction of the H-3′–O-3′ bond is not well correlated, as can be seen (see Fig. 2) by the jumps between the two gauche forms ($g+$ and $g-$) for H-2–O-2–C-2–C-1 and the $g+$ $-$ favored form for H-3′–O-3′–C-3′–C-2′. There is a significant difference between the two 3 and 3′ hydroxyl rotational preferences with the non-reducing ring preferring $g-$ and the reducing ring preferring $g+$.

Cyclomaltooligosaccharides (cyclodextrins, CDS)

α-CD. The X-ray and neutron diffraction structures of α-CD [18] are so well determined that even the hydrogen atoms are available for analysis. These data thus provide one with a critical test of an empirical force field and experimental conformational parameters are used here for that purpose. The time-averaged conformation of α-CD in vacuo was described previously [2]. Here we describe the solvation studies and the conformational changes that occur upon adding water to the vacuum structure to make up this interesting carbohydrate. We have used as our guide for comparison purposes a recent crystal structure of α-CD hydrate [18], and many other crystal structures are reviewed elsewhere [19].

In the crystal structure [18], α-CD assumes a relaxed round shape stabilized by all six possible O-2(n)···O-3($n+1$) intramolecular hydrogen bonds. There are four ordered water molecules, and all hydroxymethyl groups are *gg*. Various molecular parameters are listed in Table 2.

One must remember that the minimum and maximum values obtained from the experimental X-ray data are static values, not dynamic values. That is, they reflect the deviations between residues in the time-averaged structure obtained from analysis of the diffraction data. The calculated minimum and maximum, on the other hand, are from the retained time frames and, therefore, may not be the absolute values during dynamics. The

molecular dynamics average values do reflect an average over the dynamics time period, but again only from the retained frames (1 ps intervals). The results do not change when more frames are added to obtain the average values. With these caveats in mind, the results of this comparison are remarkable. No published simulations have reported such excellent agreement between experiment and calculation for this molecule (see for example Refs. [20,21]). Because DFT/ab initio data were fit to obtain the parameters of the AMB99C force field (experimental data were not used), it is clear that this fitting methodology is a powerful tool to obtain high-quality force fields, even without adding new functional equations or lone-pair electron positions to fit more variables. Clearly, one requires correct partial atomic charges to obtain solution results of the quality reported here.

It has been shown that in the crystal environment the *gg* conformation of the ωs is favored over the *gt* conformation by a ratio of 3.5:1 [22]. The result of the solution simulations reported here is that the *gt* form predominates with four to five groups on average *gt* and one to two on average *gg*. The molecule is generally in the round 'relaxed' shape suitable to form an inclusion complex, although the stabilization is not simply the interaction of six intramolecular hydrogen bonds.

β-CD. Results of a 100 ps dynamic simulation of β-CD in a box (the size and shape of the crystallographic unit cell) of TIP3P water molecules are given in Table 3 and Fig. 4. As one compares the X-ray crystal structure [23–25] with the vacuum and solvated states, it is clear that the ϕ and ψ values from the sol-

Table 2
Crystal structure and AMB99C dynamics (100 ps) averaged (20–102 ps) structural parameters of α-CD in a box of dimensions ($20\times20\times15$ Å) filled with TIP3P water molecules

		Crystal structure Ref. [18]	AMB99C (dynamics averaged)	AMB99C (minimized [a])
Torsion angles φ (°)				
O-4(n)–C-1(n)–O-4($n-1$)–C-4($n-1$)	Ave	170.2	171.9	171.4 [b]
	Min	161.1	149.0	165.2
	Max	−179.8	179.0	177.1
Torsion angles ψ (°)				
C-1(n)–O-4($n-1$)–C-4($n-1$)–O-4($n-2$)	Ave	−172.2	−173.6	−173.3 [b]
	Min	−165.8	−141.0	−159.9
	Max	−175.8	−183.0	−183.6
Angles (°)				
O-4(n)–O-4($n-1$)–O-4($n-2$)	Ave	119.9	120.0	120.0
	Min	116.9	110.0	117.9
	Max	122.3	129.4	122.4
Distances (Å)				
O-4(n)–Oi4($n-1$)	Ave	4.24	4.23	4.29
	Min	4.16	3.97	4.26
	Max	4.30	4.52	4.34
Distances (Å)				
O-2(n)–O-3($n-1$)	Ave	2.98	2.90	2.97
	Min	2.90	2.74	2.89
	Max	3.15	3.51	3.31
O-4–O-4 (cavity diameter)	8.31–8.60		8.2–8.9 (ave 8.5)	8.5–8.7 (ave 8.6)

[a] Minimization of the 100 ps frame of the solvated cell plus molecule, to a gradient of <0.001 kcal/Å. The min and max values in this column are for the minimized structure only.

[b] The equivalent ϕ_H and ψ_H values are ~-13 and $+13°$, respectively.

Table 3
Crystal structure and AMB99C dynamics (100 ps) averaged structural parameters of β-CD in a box of unit cell dimensions ($21.617 \times 10.026 \times 14.891$ Å, $\beta = 112.52°$) filled with TIP3P water molecules

		Crystal structure Refs. [23,24]		AMB99C (dynamics average) [a]		AMB99C (minimized [b]) [a]
Torsion angles ϕ (°)	Ave	109.9	109.8	106.6	110.8[c]	102.4 [d]
O-5(n)–C-1(n)–O-4($n-1$)–C-4($n-1$)	Min	102.5	102.3	81.0		
	Max	120.0	118.6	128.0		
O-4(n)–C-1(n)–Or($n-1$)–C-4($n-1$)	Ave	168.9		166.7	161.6	
	Min	161.0		160.2		
	Max	177.8		176.4		
Torsion angles ψ (°)	Ave	128.3	127.6	126.9	126.0 [c]	131.3 [d]
C-1(n)–O-4($n-1$)–C-4($n-1$)–C-3($n-1$)	Min	115.2	114.2	92.0		
	Max	139.9	140.4	146.0		
C-1(n)–O-4($n-1$)–C-4($n-1$)–O-4($n-2$)	Ave	−171.1		−175.3		−167.3
	Min	−160.7		−125.4		
	Max	−184.2		−199.0		
Angles (°)	Ave	128.3	128.3	128.2		126.7
O-4(n)–O-4($n-1$)–O-4($n-2$)	Min	123.8	125.2	110.6		
	Max	134.4	132.5	140.6		
Distances (Å)	Ave	4.364	4.385	4.49		4.46
O-4(n)–O-4($n-1$)	Min	4.201	4.267	4.29		
	Max	4.502	4.499	4.71		
Distances (Å)	Ave	2.857	2.884	3.10	2.87 [c]	3.27
O-2(n)–O-3($n-1$)	Min	2.768	2.801	2.38		
	Max	2.955	2.978	4.51		
C-1(n)–O-1(n)–C-4($n-1$)	Ave	117.7		119.3		118.7

[a] Includes tilted residue.
[b] Minimization of the 100 ps frame to a gradient of <0.01 kcal/Å.
[c] Does not include tilted residue.
[d] The equivalent φ_H and ψ_H values are -13.4 and $+12.9°$, respectively.

vated averages are closer to experimental values than were the vacuum average values (see Table 4, Ref. [2]). The average solvated ϕ and ψ values are ~ 3–$4°$ from the X-ray crystal structure, which is an excellent result considering that neither crystal packing or symmetry was defined in the calculated study. The results of the β-CD are complicated by 'tilted' residues in the chain, that is those residues that point the methoxy group toward the center of the molecule have dihedral angles that change the overall average.

The data in Table 3 are of interest for several reasons. First, the average dihedral angles are closer to the crystallographic values when determined in solution than in vacuum (see Ref. [2]). In fact, the O-4(n)–O-4($n-1$)–O-4($n-2$) angle remained close to the experimentally determined value, even though the average dihedral angles changed upon solvation. This suggests that the angle defined by O-4(n)–O-4($n-1$)–O-4($n-2$) is not a particularly good criterion of fit to observed structural parameters. Secondly, unlike previous calculations on β-CD [26] using the GROMOS force field and TIP3P waters in a box with dimensions of $22.1 \times 23.1 \times 25.1$ Å, we do not see a large distribution of ϕ and ψ dihedral angles. Rather, the variance of observed dihedral angles remains close to the experimentally determined structure with no bimodal distribution. The spread in ϕ values calculated with solvent is $\sim 45°$ relative to the spread in solid-state ϕ values of $\sim 18°$ (these are not vibrational amplitudes, only differences in measured values), while the spread in calculated ψ values is $\sim 54°$ compared with the solid-state spread of $\sim 26°$. These results are reasonable in that one expects more flexibility in solution than in the solid state where

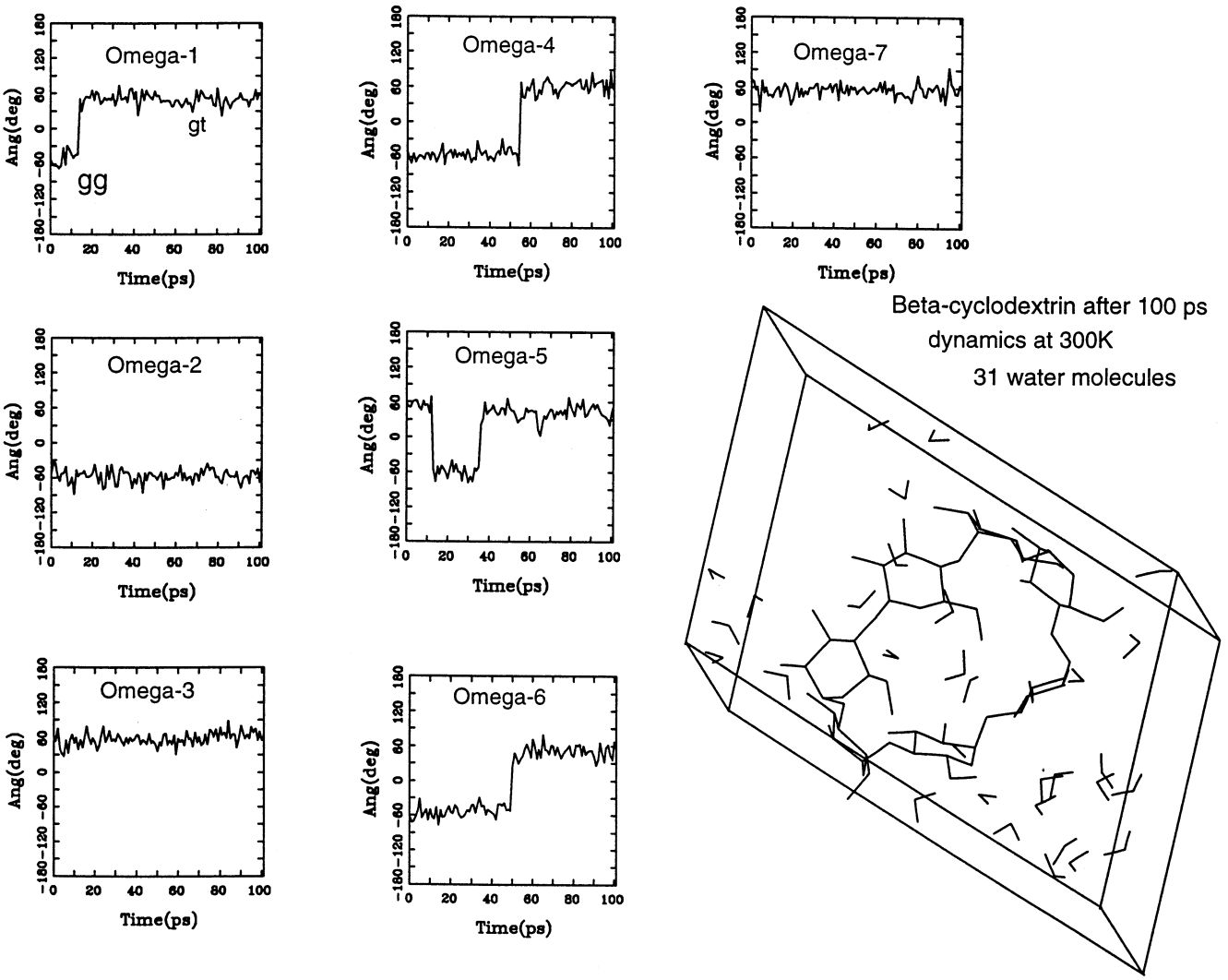

Fig. 4. Water–β-cyclodextrin dynamics analysis showing the seven dihedral angles (ωs) vs. time. The dynamics run time was 100 ps.

Table 4
Experimental X-ray and calculated average (10–100 ps) backbone dihedral angles, O-4–O-4′ distances, and C-1–O-1–C-4′ angle for γ-CD from 100 ps dynamics simulation in a box of water ($20 \times 20 \times 12$ Å) at 300 K

	AMB99C		Crystal structures [a]	
	Average dihedral angle(°)		Average dihedral angle(°)	
	Phi(ϕ)	Psi(ψ)	Phi(ϕ)	Psi(ψ)
	O-4–C-1–O-4′–C-4′	C-1–O-4′–C-4′–O-4″	O-4–C-1–O-4′–C-4′	C-1–O-4′–C-4′–O-4′
	166(168) [b]	−171(−172) [b]	165	−169
Average distance (Å) O-4–O-4′	4.50(4.49) [b]		4.50(4.48) [c]	
Average angle (°) C-1–O-1–O-4′	118(119) [b]		117(112.6) [c]	

[a] Ref [28].
[b] 100 ps simulation in a box of TIP3P water.
[c] Ref [29].

close molecular contacts make the probability of large-amplitude motions remote. Further, in both states, the spread in ψ is greater than the spread in ϕ by a similar amount. Thirdly, the dynamics simulation resulted in all but one of the ω dihedral angles in the *gt* conformation (see Fig. 4), although the X-ray structure has three *gg* and four *gt* conformations. The simulation was started with four *gg* and three *gt* conformations. Longer simulations on other cyclodextrins show similar *gg*/*gt* populations. It appears that the solvent helps maintain the nearly cyclic structure, since Lipkowitz [27] found that somewhat long and narrow structures were preferred in vacuo, although his [27] result may have more to do with the force field used than stress in the molecule. We do not find a wide range of structural differences as the simulation proceeds, although the molecule is very flexible during dynamics and could assume different shapes. A review of published studies using molecular mechanics and dynamics simulations on β-CD can be found in the Lipkowitz [19] review.

γ-CD. The cyclodextrin octamer (γ-CD) was placed in a box, $20 \times 20 \times 20$ Å, at a density of 1.002 g cm^{-3}. The simulation was run for 100 ps at 300 K. The average calculated O-4(n)–O-4($n-1$) distance was found to be 4.49 Å, and this compares very favorably with the experimental average of $\sim$4.50 Å. Other averages are complicated by residues being 'flipped' relative to the standard dihedral angles. For example, the O-4(n)–O-4($n-1$)–O-4($n-2$) angle preceding a 'flipped' residue has a maximum of 159° and a minimum of 126°, while for the angle after the flipped residue the maximum is 121° with a 90° minimum value. Even considering this question of residue flips, the average dynamic O-4(n)–O-4($n-1$)–O-4($n-2$) angle was found to be 132°, and this compares favorably with the experimental average value of 135° [24]. The O-2(n)–O-3($n-1$) distance is another parameter that can be compared with experiment if one omits the values from the flipped residues. The average calculated value (omitting two long values from flipped residues) is 2.9 Å, as compared with the experimental [24] value of 2.82 Å. Clearly, looking only at average values for these molecular parameters is not overly productive when 'flipped' conformations are involved. Dihedral angles and other parameters for two averaged dynamics structures are compared with the experimental values [28,30] in Table 4.

ε-CD (CA10). The ε-CD molecule (of DP 10) was placed in a box, $25 \times 25 \times 10$ Å, at a density of 1.001 g cm^{-3} and appropriate distance constraints and explicit images. It was observed during the 102 ps simulation that the dihedral angles of the backbone are relatively stable over time, with the most fluctuation occurring at those residues preceding the band flip residues. Average values for ϕ and ψ over a 5–102 ps run were $\phi = 98.9°$ ($\delta = +10, -12$) and $\psi = 105.4°$ ($\delta = +8, -15$), where δ values are the maximum and minimum values observed excluding the band-flipped residues. These values compare favorably with the X-ray diffraction average values [24] of $\phi = 99°$ ($\delta = +3, -5$) and $\psi = 106°$ ($\delta = +16, -10$), also excluding the flipped residues. The average of the two band-flip dihedral angles (calculated, 96°, −75°) compare favorably with the observed values (84°, −65°). The agreement is very good given the crystal packing forces (the small cell thickness does allow molecule-to-image-molecule interactions although not in the correct symmetry positions) were not created from the unit cell dimensions in the simulation. The average O-4(n)–O-4($n-1$) value over the 5–102 ps of the simulation was 4.36 Å, somewhat shorter than the observed [24] value of 4.49 Å. The average O-4(n)–O-4($n-1$)–O-4($n-2$) angle was found to be 138.1° from the simulation. This value compares favorably with the observed [24] value of 138.2°. Also of interest are the number of water molecules interacting with ε-CD through hydrogen bonding during the simulation. Over the time (5–102 ps) of the simulation (contacts calculated every picosecond) it was found that on average three hydrogen bonds/residue were observed from the contact of water with the ε-CD molecule (see Fig. 5 for explanation of contact criteria). X-ray analysis of ε-CD showed that crystallization from aqueous solutions resulted in a 20.3 hydrate, or $\sim$two hydrogen-bonded water molecules/residue. The crystal packing does not allow more water interactions, so we believe that the calculated hydration number is quite reasonable.

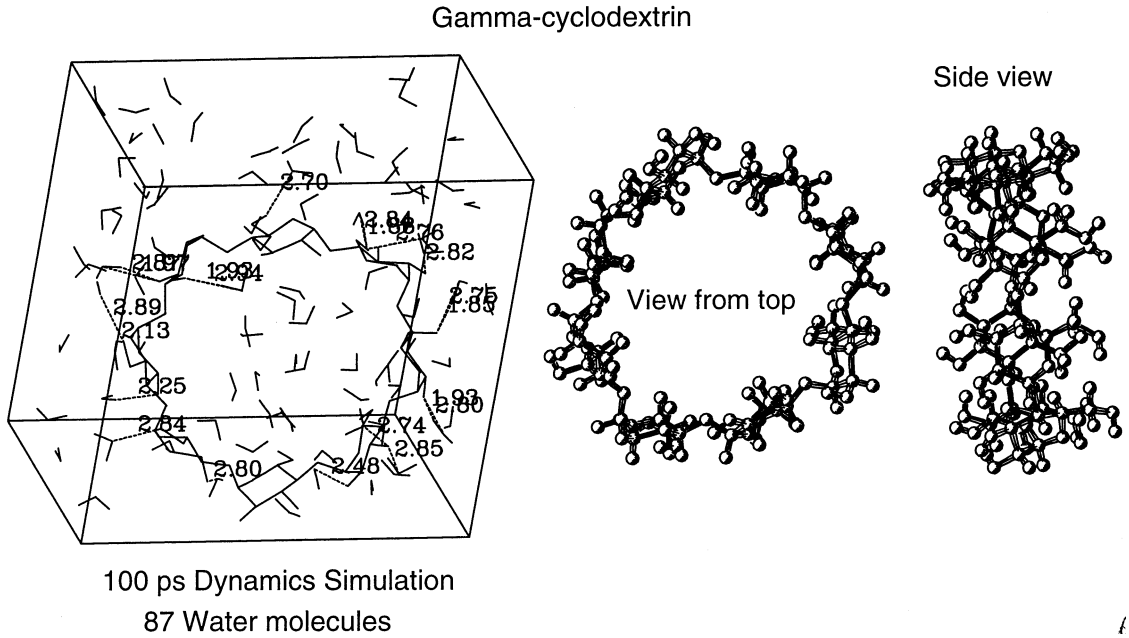

Fig. 5. Water–γ-cyclodextrin dynamics simulation showing the water molecules in contact with the γ-cyclodextrin molecule at frame 96 of the dynamics run. The average number of water molecules in contact with each residue is obtained by counting contacts (defined as those O–O interactions within 3.5 Å and O···H–O angle greater than 120°) for each frame and dividing by 8 to get number of water molecules/residue.

CA21. One cyclomaltooligosaccharide, compound CA21 of DP 21, was recently characterized by means of small-angle X-ray scattering (SAXS), An experimental radius of gyration (R_G) of 11.5 Å was obtained [30]. The authors [30] used molecular modeling to obtain a three-turn single-helical form, whose R_G was in agreement with the scattering data. The CA21 molecule was generated by linking glucose units to make α-(1→4)-D-glucan chains of 21 units. Creation of the cyclic structure was carried out using a mild distance constraint between the first and 21st residues, while a short dynamics simulation was carried out. This method allowed the ring structure to form without stress on the bridge dihedral angles and without distorting any glucose chair ring structure. It was found that by starting the structure generation with the dihedral angles chosen in the low-energy region of the allowed β-maltose conformational space, a large ring structure was automatically produced, which placed the first and last residues within several Ångstroms of one another. Thus, adding the distance constraint produced only slight stress on the molecule and allowed the closing of the bridge without distortion. The result was a nearly perfect circular structure with the normal maltose twist as one proceeds around the ring.

The cyclic structure was placed in a box, 30 × 30 × 30 Å, with 728 water molecules added as described previously, resulting in a density of 1.016 g cm^{-3}. Distance cut-offs starting at 14 Å and slowly changing to 16 Å before termination were applied, and the explicit image method used with one cell layer generated in the x, y, and z directions. Energy minimization was carried out for 500 cycles of conjugate gradient, and 102 ps of dynamics at 300 K was carried out. Data were calculated at 1 fs time steps, and the data were collected and stored every picosecond. The stability of the energy was checked routinely for drift as the calculation proceeded. No constraints were applied to any atoms during the simulation. A second run of 102 ps was carried out on the energy-minimized form of the final structure of the previous run.

The radius of gyration, R_G, was evaluated [30] from the scattering data from the initial slope of the Guinier plots $\ln I(q)$ versus q^2, according to the Guinier approximation [32], as shown in Eq. (5):

$$I(q) \text{a} \exp(-R_G^2 q^2/3) \quad (5)$$

R_G was evaluated as 11.3–11.5 Å over a polymer concentration range of 3–19 mg/mL. The thickness of the molecule in solution was estimated to be 10.4 Å [30].

Results of two molecular dynamics simulations on the solvated CA21 of cycloamylose are given in Table 5. The calculated R_G values were obtained using the Amorphous Cell module of the Polymer programs from MSI. The result of the final frame of dynamics from run I was somewhat higher than the SAXS value, while the final frame of the second run was somewhat lower than the SAXS value. Upon removal of the water and energy minimization to remove close contacts, the average dihedral angles remained close to those shown but the R_G value dropped slightly to 9.8 Å.

It was observed in a preliminary dynamics simulation that the original AMBER force field [5] allowed the cycloamylose, CA21, to collapse from the nearly circular starting form to a densely folded form with no observable repeatable secondary structure. Analysis of the resulting structure indicated two problem areas needing correction. The first was the creation of several skewed-boat residues, the second was the occurrence of several bridge dihedral angles, which were in the 'flipped' locations on the (ϕ_H, ψ_H) map allowing very tight turns to occur. Both of these problems have been corrected in the modifications made to give the AMB99C force field [2]. For example, the torsional potentials for the six-membered sugar rings were modified (see Ref. [2], Appendix A) and appear to prevent the skewed-boat formation from forming easily, although it is still possible if sufficient strain is applied. Secondly, the barrier between the allowed low-energy regions and the abnormal or 'flipped' regions of conformational space were elevated to prevent easy access to this region during room temperature simulations. The latter was a result of the DFT/ab initio study, where energy differences of several kilocalories for the 'flipped' conformations relative to the global minimum were found [1]. Subsequent simulations with AMB99C resulted in structures stable against skew formation or 'flipped' transitions over hundreds of picoseconds of dynamics at room temperature, and resulted in R_G values close to those found experimentally (see Table 5). One of the structures found appears as a twisted three-lobed cloverleaf-like formation (see Fig. 6), in general agreement with the conclusions of Kitamura et al. [30]. The pseudo ring loop sizes range from $\sim$11 to $\sim$13 Å across with loop spacing of $\sim$six residues. Using standard conditions (see Fig. 5) for evaluating hydrogen bonding, we find approximately 4.4 water molecules interacting (1.91–2.49 Å, H–O distance) with each glucose residue and 18 intramolecular hydrogen bonds (1.81–2.13 Å, H–O distance) in the 21-mer. These results are also in good agreement with Kitamura et al.'s calculations using the GROMOS force field [30]. Of interest is the observation that during dynamics visualization it was noted that the molecule was undergoing a conformational transition in which one lobe would be similar to a 6–7-residue V-helix loop, a second lobe would look similar making a gourd shape, and the third lobe would be turned approximately 90° to the other two, turning in six residues with the ends of the turn closer to one another relative to the other two lobes. As the transition took place the lobes changed, the tight lobe getting looser, while one of the loose (gourd-shaped) lobes became tighter. This was a continuous transition during the time course of the simulation. It is not clear what implica-

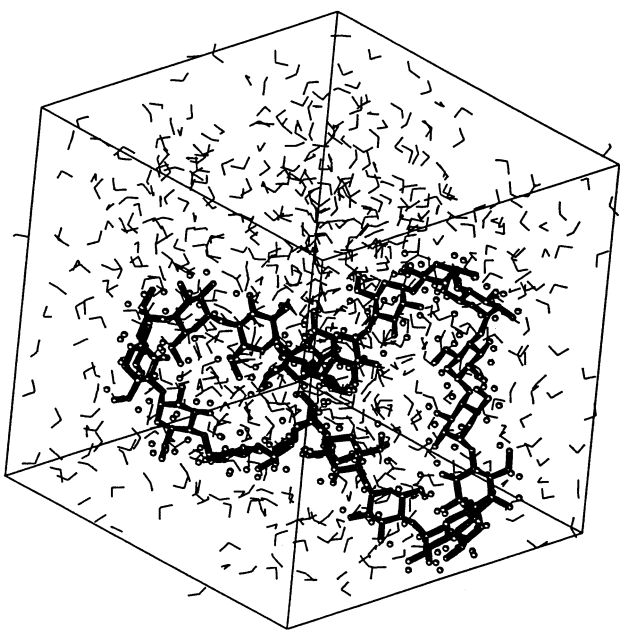

Fig. 6. One pictorial vision of the CD21 molecule after dynamics simulation run I.

Table 5
Results of calculations and experimental values of radius of gyration and dihedral angles of CA21 using AMBER and the AMB99C force fields

	AMBER	AMB99C I	AMB99C II	SAXS [30]	α-Cyclodextrin Ref. [31]	Amylose-V_6 Ref. [33]	Amylose A Ref. [34]
Radius of gyration, R_G, (Å)	9.5	11.2	11.5	11.3–11.5			
Average dihedral (ϕ_H, ψ_H) angles from frame 102 (°)	NA [a]	(−20, −12) [b]	(−14, −10) [b]		NA [a] (−32, −4)	NA [a] (−14, −8)	NA [a] (−25, −32)

[a] NA = not available or not calculated.
[b] Average ϕ_H and ψ_H dihedral angles for all 21 residues from dynamics frames over the times 10–102 ps (I) and 5–200 ps (II) from two different simulations using different starting structures.

tions one may glean from this observation, but it is of interest to note that these changes did not significantly change the value of R_G. In a second dynamics simulation of 85 ps with the TIP3P water model, one residue moved into the 'flipped' conformational state at 45 ps, and remained in that conformational state for the remainder of the simulation. However, this conformational change did not collapse the structure, which retained a radius-of-gyration, $R_G = \sim 11$ Å, in agreement with those given in Table 5. A third 200 ps simulation produced a more open structure but the R_G value, given in Table 5 as Conformer II, remained at 11.5 Å. Clearly, the R_G value can be obtained with different conformations and must be considered only a guide to conformation preference.

The average dihedral angles obtained from the dynamics run listed in Table 5 are in general agreement with various experimental X-ray and NMR results, as given in Table 5. From the ^{13}C NMR spectrum, Kitamura et al. [30] suggested that the chemical shifts are very similar to those of the corresponding resonances of linear amylose. The average dihedral angles obtained here would be in agreement with that assessment as they are close to those obtained for amylose V_6 and amylose A.

4. Conclusions

Results presented here confirm the utility of the AMB99C potentials for use in α-(1→4)-bridged carbohydrate studies. Several novel results have come out of this study and are being explored more fully. Clearly, the use of explicit solvent molecules has eliminated some of the historical problems associated with vacuum calculations and the intricate network of intramolecular hydrogen bonds. The competition for electrostatic interactions is balanced between intra- and intermolecular interactions and this allows the exocyclic hydroxyl group hydrogens to be nearly freely rotating rather than strongly directed toward the nearest donor or acceptor atom. Using boxes filled with water, explicit images with infinite lattice conditions, and by adjusting the density and

pressure, we have carried out many simulations of the disaccharide maltose and larger cyclic molecules, such as the CA21 cyclomaltooligosaccharide. The results are in excellent agreement with available experimental results. It is apparent that one must carry out simulations on large systems to test empirical potentials for ring collapse and abnormal conformational jumps. This is irrespective of how well one reproduces ab initio geometries and energies on model systems. To this end the experimental X-ray structures and radius of gyration values were very useful as testing parameters. The newly derived force field, AMB99C, has corrected deficiencies found in previous versions of AMBER and closely simulates experimental structural carbohydrate parameters. Preliminary calculations on amylose A- and B-form double helices and amylopectin bridged double helices are presented elsewhere [35].

References

[1] F.A. Momany, J.L. Willett, *J. Comput. Chem.*, submitted for publication.
[2] F.A. Momany, J.L. Willett, *Carbohydr. Res.*, 326 (2000) 194–209.
[3] IUPAC-IUB Commission on Biochemical Nomenclature, *J. Mol. Biol.*, 52 (1970) 1–17; *Arch. Biochem. Biophys.*, 145 (1971) 405–421; *Eur. J. Biochem.*, 18 (1971) 151–170.
[4] S.W. Homans, *Biochemistry*, 29 (1990) 9110–9118.
[5] W.D. Cornell, P. Cieplak, C.I. Bayly, I.R. Gould, K. Merz Jr., D.M. Ferguson, D.C. Spellmeyer, T. Fox, J.W. Caldwell, P.A. Kollman, *J. Am. Chem. Soc.*, 117 (1995) 5179–5197.
[6] J.O. Duus, K. Bock, S. Ogawa, *Carbohydr. Res.*, 252 (1994) 1–18.
[7] T. Peters, B. Meyer, R. Stuike-Prill, R. Somorjai, J. Brisson, *Carbohydr. Res.*, 238 (1993) 49–73.
[8] A.S. Shashkov, G.M. Lipkind, N.K. Kochetkov, *Carbohydr. Res.*, 147 (1986) 175–182.
[9] M.J. Gidley, in G.O. Phillips, P.A. Williams, D.J. Wedlock (Eds.), *Gums Stab. Food. Ind. 4*, Proc. 4th Int. Conf., IRL, Oxford, UK, 1988, pp. 71–80.
[10] I. Tvaroska, M. Hricovini, E. Petrakova, *Carbohydr. Res.*, 189 (1989) 359–362.
[11] B. Mulloy, T.A. Frenkiel, D.B. Davies, *Carbohydr. Res.*, 184 (1988) 39–46.
[12] K. Ott, B. Meyer, *J. Comput. Chem.*, 17 (1996) 1068–1084.
[13] K. Ott, B. Meyer, *Carbohydr. Res.*, 281 (1996) 11–34.
[14] T.M. Glennon, T.-J. Zheng, S.M. LeGrand, B.A. Shutzberg, K.M. Merz Jr., *J. Comput. Chem.*, 15 (1994) 1019–1040.
[15] J.W. Brady, R.K. Schmidt, *J. Phys. Chem.*, 97 (1993) 958–966.
[16] W. Damm, A. Frontera, J. Tirado-Rives, W.L. Jorgensen, *J. Comput. Chem.*, 18 (1997) 1955–1970.
[17] T. Weimer, U.C. Kreis, J.S. Andrews, B.M. Pinto, *Carbohydr. Res.*, 315 (1999) 222–233.
[18] R. Puliti, C.A. Mattia, L. Padiano, *Carbohydr. Res.*, 310 (1998) 1–8.
[19] K.B. Lipkowitz, *Chem. Rev.*, 98 (1998) 1829–1873.
[20] J.E.H. Koehler, W. Saenger, W.F. van Gunsteren, *Eur. Biophys. J.*, 15 (1987) 197–210.
[21] J.E.H. Koehler, W. Saenger, W.F. van Gunsteren, *J. Mol. Biol.*, 203 (1988) 241–250.
[22] F.W. Lichtenthaler, S. Immel, *Justus Liebigs Ann. Chem.*, (1996) 27–37.
[23] K. Linder, W. Saenger, *Carbohydr. Res.*, 99 (1982) 103–115.
[24] W. Saenger, J. Jacob, K. Gessler, T. Steiner, D. Hoffman, H. Sanbe, K. Koizumi, S.M. Smith, T. Takaha, *Chem. Rev.*, 98 (1998) 1787–1802.
[25] T. Aree, W. Saenger, P. Leibnitz, H. Hoier, *Carbohydr. Res.*, 315 (1999) 199–205.
[26] M. Prabhakaran, *Biochem. Biophys. Res. Commun.*, 178 (1991) 192–197.
[27] K.B. Lipkowitz, *J. Org. Chem.*, 56 (1991) 6357–6367.
[28] K. Harata, *Bull. Chem. Jpn.*, 60 (1987) 2763–2767.
[29] K. Linder, W. Saenger, *Biochem. Biophys. Res. Commun.*, 92 (1980) 933–938.
[30] S. Kitamura, H. Isuda, J. Shimada, T. Takada, T. Takaha, S. Okada, M. Mimura, K. Kajiwara, *Carbohydr. Res.*, 304 (1997) 303–314.
[31] P.C. Manor, W. Saenger, *J. Am. Chem. Soc.*, 96 (1974) 3630–3639.
[32] G. Porod, in O. Glatter, O. Kratky (Eds.), *Small Angle X-ray Scattering*, Academic Press, London, 1982, pp. 17–51.
[33] G. Rappenecker, P. Zugenmaier, *Carbohydr. Res.*, 89 (1981) 11–19.
[34] H.C.H. Wu, A. Sarko, *Carbohydr. Res.*, 61 (1978) 7–25.
[35] F.A. Momany, J.L. Willett, ANTEC99, Plastics-Bridging the Millennia, *Proc. SPE 57th Ann. Tech. Conf.*, 1999, pp. 2402–2406.